Hindawi Publishing Corporation
Journal of Nanomaterials
Volume 2011, Article ID 157690, 16 pages
doi:10.1155/2011/157690

Review Article

Synthesis and Characterization of 1D Ceria Nanomaterials for CO Oxidation and Steam Reforming of Methanol

Sujan Chowdhury and Kuen-Song Lin

Department of Chemical Engineering and Materials Science and Fuel Cell Center, Yuan Ze University, Chung-Li 320, Taiwan

Correspondence should be addressed to Kuen-Song Lin, kslin@saturn.yzu.edu.tw

Received 12 June 2011; Accepted 29 July 2011

Academic Editor: Yanqiu Zhu

Novel one-dimensional (1D) ceria nanostructure has been investigated as a promising and practical approach for the reforming of methanol reaction. Size and shape of the ceria nanomaterials are directly involved with the catalytic activities. Several general synthesis routes as including soft and hard template-assemble phenomenon for the preparation of 1D cerium oxide are discussed. This preparation phenomenon is consisting with low cost and ecofriendly. Nanometer-sized 1D structure provides a high-surface area that can interact with methanol and carbon-monoxide reaction. Overall, nanometer-sized structure provides desirable properties, such as easy recovery and regeneration. As a result, the use of 1D cerium has been suitable for catalytic application of reforming. In this paper, we describe the 1D cerium oxide syntheses route and then summarize their properties in the field of CO oxidation and steam reforming of methanol approach.

1. Introduction

Modern society insists on a new energy carrier with the chemical conversion of fuels to minimize the environmental disaster. Recently, hydrogen production processes have applied effectively for environmental impact and energy generation issues. Hydrogen is usually generated through the organics mainly based on hydrocarbon waste treatment and is extremely renowned as a clean energy carrier [1–6]. Nowaday, it is an important environmental issue on the case of an atmospheric condition. Methanol is one of the most promising sources of hydrogen for fuel cell applications included with the advantages of high-energy density, easy availability, and safe handling/storage materials [3]. In the literatures, several types of catalyst are frequently used for hydrogen generation by steam reforming of methanol (SRM) [1, 5, 6]. SRM is the main reforming reaction that provides the stoichiometric conversion of methanol to hydrogen. The overall methanol decomposition reaction can be regarded as the effect of the conversion of CO, CO_2, H_2O, and water gas shift (WGS) reaction. SRM is one of the attractive approaches on the rise owing to higher-energy density and relatively low-reforming temperatures (200–300°C). Combination of SRM and partial oxidation of methanol (POM) is effectively known as autothermal reforming (ATR) process and is attenuated with decreasing the reactor volume and design [3, 7, 8]. SRM is the main reforming reaction that provides the stoichiometric conversion of methanol to hydrogen. In addition, methanol steam reforming produces a relatively small amount of carbon monoxide at a low temperature, whereas carbon monoxide is known to be very poisonous for Pt catalyst in a proton exchange membrane fuel cell (PEMFC) system [5]. Therefore, there has been considerable interest in the development of catalytic performance of methanol decomposition. The catalytic reaction for SRM and ATRM is generally based on copper or palladium. As well, cerium-promoted copper catalyst existed for the recovery of hydrogen from methanol with the optimization of carbon monoxide concentration [2–4]. Cerium is often referred to as the rare-earth element or lanthanide ($Z = 57$–71). As an important component in catalysts, ceria ($Z = 58$) promotes high oxygen storage capacity (OSC), oxygen ion conductivity, and oxygen vacancy. The formation of oxygen vacancy can be expressed by the following equation:

$$\frac{4Ce^{4+}_{(s)} + O^{2-}_{(s)} \longrightarrow 4Ce^{4+} + 2e^{-}}{V_{(o,s)} + (1/2)O_2 \longrightarrow 2Ce^{4+}, 2Ce^{3+}_{(s)} + V_{(o,s)} + (1/2)O_2}, \quad (1)$$

where $V_{(O,s)}$ represents an empty position (anion-vacant site) originating from the removal of O^{2-} from the lattice. Charge balance is maintained by the reduction of two cerium cations from +4 to +3. The radius of the Ce^{3+} ion (1.14 Å) is larger than that of Ce^{4+} (0.97 Å), and hence the lattice expansion is a consequence of the reduction of Ce^{4+} ions to Ce^{3+}. There is a gradual decrease in the concentration of oxygen vacancies extended from the surface to the bulk. Such gradient enables the outward diffusion of lattice oxygen to the surface. Therefore, the reduction of Ce^{4+} to Ce^{3+} by oxygen ion leads to the generation of surface oxygen vacancy. These oxygen vacancies can be acted as promoting sites for NO and CO conversion [1–9].

As well, cerium oxide (CeO_2) is commonly known as cerium dioxide, ceria, or ceric oxide, visualized as pale yellow-white powder and slightly hygroscopic in nature at the atmospheric conditions. Usually ceria are obtained through the calcinations of cerium oxalate or cerium hydroxide. In the room temperature and pressure, CeO_2 represents much more stable form than cerium (III) oxide (Ce_2O_3). CeO_2 has consisted of FCC crystal fluorite structure, and their Ce^{4+} ions are closed packed and O ions in the space of a tetrahedron. It has been evident that doped metal ions onto the ceria material are still showing the FCC crystal structure [10, 11]. Novel structure of 1D ceria nanostructure with various morphologies such as nanorods, nanowires, nanotubes, and nanopolyhedrons has been successfully fabricated by a variety of methods [12–28]. Nanoscale ceria materials of 1D structure are represented with surface morphologies, allowing attractive applications for catalytic reactions [12, 13]. Moreover, ceria nanomaterial research has focused on the scheme of the physical treatment, based on the controlling of the reaction time, temperature, pressure, and so forth.

Ceria is belonging to higher oxygen ion conductivity and one-dimensional ceria, and doped ceria have wide applications in the electrochemistry, catalysis, optics, and different fields [14–23, 27, 28]. Therefore, as synthesized one-dimensional ceria nanomaterials are particularly attained an attraction for the catalytic behavior on the chemical reaction of carbon monoxide and methanol, which are overviewed in this paper. General physical and chemical properties of the ceria nanomaterials are specifically enhanced through the dimension of the nanostructure and doped material with respect to their bulk-like materials.

2. Nucleation and Growth

Bulk- or nanometer-sized different dimensional crystal structure growth is readily involved in the process of precipitation of solid phase from solution. Simultaneous process of nucleation and following growth phenomenon govern the crystal morphology (as including size and shape) in the precipitation reaction. At the initial stage, numerous small crystallites are formed to refer to as the nucleation process. Consequently, small crystallites are aggregated together to form thermodynamically stable structure and refered to as a growth process. An effective process control is leading to the formation of the desired solid crystal structure. Thus, the formation of crystal structure is essential to consider the nucleation and growth of structure. Initially, surface energy plays an important role to increase the size of the nuclei where nucleation is a spontaneous process, and large crystals have lower surface energy. Surfactant, solvent, concentration, pH, reaction temperature, and time are readily involved in the surface energy of the crystal growth. In the thermodynamic point of view, addition of surfactants is used to control the process of nucleation and the size of the resulting nucleus. Nucleation process is readily involved in heterogeneous nucleation, secondary nucleation and homogeneous nucleation. Presence of suspended particles may provide the start of the nucleation, and thus insists the heterogeneous nucleation with the requirement of less energy. Heterogeneous nucleation obtains more often than homogeneous nucleation. Secondary nucleation is involved in the formation of nuclei with the recombination of existing crystal. On the other hand, homogeneous nucleation occurs spontaneously and randomly in the absence of solid interface by a combination of solute molecules. The growth process of crystal occurs for dissolving the solute in the solution at higher temperatures and then cooling to low temperature or by adding the necessary reactants to produce a supersaturated solution during the reaction. This overall crystal growth phenomenon is belonging to the consumption of smaller particle by larger particle to form larger stabilized structure, and it has been referred to as Ostwald ripening also known as coarsening [29]. Lifshitz and Slyozov first developed mathematical derivation of Ostwald ripening process and independently by Wagner; their combined models today are referred to as LSW theory. The relationship between monomer concentration and crystal size is established by the Gibbs-Thomson equation with the Fick's First Law and Einstein-Stokes equation as follows:

$$\begin{aligned} \overline{r}^3 - \overline{r_0}^3 &= Kt, \\ \overline{r}^3 - \overline{r_0}^3 &= \frac{8\gamma V_m^2 C_{r=\alpha} D}{9R_g T} t, \\ \overline{r}^3 - \overline{r_0}^3 &= \frac{8\gamma V_m^2 C_{r=\alpha}}{54\pi\eta a N_A} t, \end{aligned} \tag{2}$$

where $\overline{r}$ is an average particle radius, $\overline{r_0}$ is an initial average particle radius, $C_{r=\alpha}$ is the solubility of the particle material, V_m is the molar volume of the particle material, D is the diffusion coefficient ($k_B\,T/6\pi\eta a$) of the particle material, R_g is the ideal gas constant, T is the absolute temperature, t is the time, k_B is Boltzmann's constant (R_g/N_A), η is the viscosity, a is the ionic radius of the particle, and N_A is the Avogadro constant. Thus, cubic of the average radius of the precipitate particles is a function of time, that is, $\overline{r}^3 = Kt$, where K is the coarsening rate constant that can be obtained from the slopes of the linear regions of the plots of $\overline{r}^3$ versus time and increases with the aging temperature. The activation energy is obtained from the slope with the plots of coarsening rate constant versus inverse of absolute temperature, and it would be a straight line. Nuclei formation that precedes crystal growth can occur by solid-state restructuring of the gel or precipitation from the supersaturated solution [30, 31].

In the last decade, nuclear magnetic resonance (NMR), small-angle and wide-angle X-ray, Raman spectroscopy, and neutron scattering spectroscopy techniques have provided the details information about the nucleation process [30, 31]. Recently, Pan et al. elaborately studied specifically addressing, the coarsening of one-dimensional ceria nanoparticle growth [32].

3. Synthesis of One-Dimensional Structured Cerium Oxides

One-dimensional cerium oxides can be produced via a simple hydrothermal and precipitation route using ammonia solution and precursor. In addition, most synthesis methods for 1D structured cerium oxides employ templates (soft and hard), which assist in obtaining a uniform morphology and the desired morphological phenomenon. Crystal's structure formation is basically involved with the precipitation process then basically consists of a nucleation step followed by particle growth stages where surface tension (γ) and saturation ratio (S) are influenced by surfactants, solvent, concentration, pH ratios, and so forth. In other words, surfactant on the surface of the nucleus directly reduced the surface tension and thus caused smaller critical radius with critical energy. The presence of micelles in solution also affects the process of nucleation and growth of the crystal where micelles solubilise the molecules of the material, thus affecting the relative supersaturation towards the nucleation and growth of the crystal.

3.1. Soft-Template Techniques. Surfactant plays an effective role in the preparation of 1D nanophase compounds and has been adversely observed in the past decades [14–24, 33]. Most commonly used soft templates are surfactants, such as cetyl trimethyl ammonium bromide (CTAB), polyvinylpyrrolidone (PVP), tetrabutylammonium bromide (TBAB), and polyethylene glycol (PEG). Cerium salts (either chloride or nitrate) under basic conditions react with ammonia at room temperature which results in the precipitation of gelatinous and hydrous cerium oxide. It is well evident that the geometry of the monomer will determine the size and shape of the surfactant aggregates. The desired size and shape of this aggregation are based on the packing parameter (P) concept $P = v/a_0 l$, where packing properties of surfactant depend on the volume v of the hydrocarbon chain, average area of a hydrophilic head group a_0 (defined by the equilibrium between hydrocarbon tail attraction and head group repulsion), and the critical chain length l. The packing parameter values in the rage of $1/3 < P < 1/2$ form cylindrical micelles, values of $P < 1/3$ lead to spherical micelles, and $P > 1/2$ favors flat bilayers (lamellar sheet) as represented in Figure 1. The formation of micelle is usually nonsphericity and consists of ellipsoidal shape, oblate shape, acetabuliform, or claviform. Usually claviform shape (cylindrical micelles) is obtained in the case when the concentration of surfactant reaches ten times that of critical micelles concentration (CMC). There are many methods available in literature for the determination of the CMC: surface tension, spectrophotometric, kinetics, conductivity, osmotic pressure, and so forth [30–35]. Fluorescence spectroscopy is a sensitive technique for accurately determining the CMC. Halder used the fluorescence spectroscopy for the determination of CMC of cetyl trimethyl-ammonium bromide (CTAB) [30]. It is well known that CMC of CTAB is around 0.90–0.98.

The size and shape of the 1D nanostructure are greatly influenced through the reaction time, reaction temperature, and surfactant/Ce^{3+} ratio in the initial solution [18, 36–40]. Triangular and rhombic shape ceria nanoparticles are attained with the influence of surfactant/Ce^{3+} ratio, carbamide concentration, and reaction temperature [41, 42]. Guo et al. [42] synthesized $Ce(OH)CO_3$ triangular microplate by a thermal decomposition-oxidation process at 150°C for 16 h using surfactant/Ce^{3+} molar ratio 2 : 1, and calcination process produces straw-yellow triangular ceria microplate in air at 650°C for 7 h. Later on, Zhang et al. [41] reported the synthesis of the rhombic $Ce(OH)CO_3$ nanostructure by a sonochemical method using surfactant/Ce^{3+} molar ratio 1 : 10. Finally, rhombic ceria nanostructure is obtained by calcination at 500°C in air for 0.5 h and to remove the CTAB. They investigate that reaction temperature is lower than the boiling point of water (100°C) that can be formed the mixture of nanoparticles nanorods and irregular microrods. Therefore, reaction temperature and time also play an important role in the formation of rhombic microplates. After that, Riccardi et al. [43] used similar surfactant/Ce^{3+} concentration and conditions as proposed by Guo et al. with a slight modification of reaction environment and time. They synthesized the cerium carbonate hydroxide (orthorhombic $Ce(OH)CO_3$) hexagonal-shaped microplates with a domestic microwave (2.45 GHz, maximum power of 800 W) at 150°C for 30 min with a fixed heating rate of 10°C min^{-1} and then converted into ceria cubic/rhombus shape after a thermal decomposition oxidation process at 500°C for 1 h. They conclude that microwave method increases the kinetics of crystallization by one or two orders of magnitude compared to the conventional hydrothermal [29, 43–48]. Similarly, ceria nanocube is obtained in the presence of ethylene glycol, oleic acid, and *tert*-butylamine at the different temperatures of microwave radiation for 60 min [49]. The high-frequency electromagnetic radiation interacts with the permanent dipole of the existing liquid to initiate rapid heating from the resultant molecular rotation. Thus, the effects of the superheating environment within a short period of time concern and facilitate the crystal growth. Instead of surfactant (CTAB), there is a significant effect of urea (or carbamide) solution on the synthesis of ceria nanomaterial, and we will explain this effect in the nontemplate technique section. Vantomme et al. [17] and Pan et al. [18] reported the formation of CeO_2 nanorods with a diameter of 10–25 nm at 80–160°C by the presence of CTAB. Pan and coworkers [18] also synthesized the CeO_2 nanoplates by hydrothermal reactions with CTAB. They controlled the conversion of nanoplates into nanotubes and nanorods by using changing CTAB/Ce^{3+} ratio values, reaction time, temperature, and ammonia solution instead of carbamide. Higher temperature and higher concentration

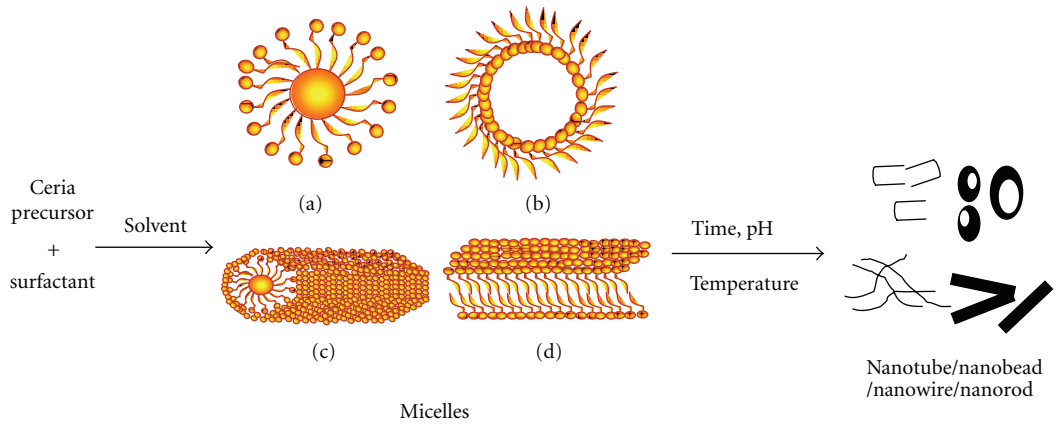

Figure 1: Different types of micelle: (a) normal, (b) reverse, (c) rodlike, and (d) bilayer structures for the formation of nanotubes, nanobeads, nanowires, and nanorods.

of CTAB as a surfactant are controlled by the synthesis of Ce-NT in the two-step procedure. In the first step, a higher concentration of the CTAB led to an increase in the absorption force between the CTA^+ and $Ce^{+3/+4}$ ion pairs and accelerated the formation of lamellar sheet as represented by the packing parameter $P > 1/2$. In the second step, Ce-NT was formed by rolling up the lamellar sheets. In addition, sthe lower concentration of CTAB can appear into a cubic plate-like structure, where reaction temperature and time controls the cubic platelike to nanoplate, hexagon, and nanorod structure, respectively. By using a precipitation method, Vantomme et al. [17] and Yan et al. [39] carried out the ceria nanowire preparation with the presence of easily available CTAB. Furthermore, Zhang et al. [24] prepared 1D ceria nanorods at room temperature in a one-step process through polyethylene glycol (PEG) surfactant and alkali solution. They confirmed that vigorous agitation without ultrasound at various temperatures (25, 40, and 60°C) would form only nanoparticles as the sole products, even with a longer reaction time. Concentration of the surfactant (e.g., PEG or CTAB) significantly affects the formation of 1D nanostructures [17, 18, 24]. Moreover, the transformation from one structure to the next is caused by intermolecular interactions between surfactant monomers. According to Ho et al. [15], ethylene glycol-mediated synthesis has been widely used for the following physical properties: (1) a high-dielectric constant, which enhances the solubility of inorganic salts; (2) a high boiling point (195°C at an atmospheric pressure), which makes it possible to carry out the preparation of inorganic compounds at relatively high temperatures; (3) its strong reducing power. Additionally, Ho et al. [15] observed that a higher precursor concentration with lower reaction time provides spherical-shaped cerium oxide increasing the reaction time, consequently extended the spherical shape into 1D rod structures. In addition, with similar experimental conditions and a lower precursor concentration, they obtained the spindle-shaped nanostructure.

Surfactants were frequently used for the fabrication of cerium oxide 1D nanowire/nanofibers. Qi et al. [22] first time demonstrated the electrospinning technique for the formation of PVP/$Ce(NO_3)_3$ composite fibers. They fabricated the cerium oxide hollow nanofibers with calcining the composite fibers at 600–800°C for 10 h. According to the FE-SEM microphotographs, the diameters of CeO_2 hollow nanofibers (300 nm at 600°C and 600 nm at 800°C, resp.) were smaller than those of PVP/$Ce(NO_3)_3$ composite fibers (1-2 μm), with the length of greater than 50 μm. They observed, through TG-DTA and FTIR data analysis, that the calcination temperatures largely influenced the formation of CeO_2 hollow nanofibers. In addition, cationic surfactant played an important role in the preparation of nanowire and nanotube. Yang and Guo [40] also employed octadecylamine ($C_{18}H_{37}NH_2$) (cationic surfactants) as the structure-directing agent to synthesize CeO_2 nanowires with a diameter of 10–25 nm in the presence of nitric acid and water, where nitric acid was used for the transformation of octadecylamine into octadecylammonium nitrate to dissolve in water. They explained that octadecylammonium cations ($C_{18}H_{37}NH_3^+$) in aqueous solution could form claviform micelles by the self-assembly. Cerium hydroxide is combined by the hydrated Ce^{+4} ions with H_2O molecules or OH^- ions and then polymerized at the micelles-solution interface to form the nanowire structure as diameters ranging between 10 and 25 nm. Yang and Guo [50] also synthesized the $Ce(OH)CO_3$ to fluorite-type Ce-NT with an outer diameter of 10–20 nm and inner diameter of 5-6 nm. $Ce(OH)CO_3$ was attained by a hydrothermal method using $Ce(NH_4)_2(NO_3)_6$ as the Ce source, octadecylamine as a surfactant template, and urea as a precipitation agent. On the other hand, cationic surfactants (i.e., alkyltrimethylammonium salts, CTAB, octadecylamine, or ethylenediamine ($C_2H_4(NH_2)_2$)), hydrous cerium oxide can incorporate the organic molecule by exchange with surface OH^- groups with the formation or reverse micelle. This approach follows the observation that hydrous oxides can exchange either cations or anions, depending on the pH of the medium [36, 37]. If the pH is higher than that of the isoelectric point of hydrous cerium oxide (6.75–8, depending on the environment), then incorporation of cationic surfactants takes place.

Reverse micelle is another process to the synthesis of different structure in the presence of the reaction media. Significant surfactant solutions in organic solvents are capable of solubilizing water in the polar core and are called as reverse micelles as shown in Figure 1. It seems that water can be readily incorporated in the core of the micelle, with the radius of the micelle increasing as the water/surfactant ratio increases. Reverse micelles provide spontaneous self-assembly of surfactants in solution for the formation of nanorods as specially in the presence of anionic surfactant sodium bis(2-ethylhexy) sulfosuccinate (AOT). Kuiry et al. [51] reported that the cylindrical supra-aggregates and their subsequent growth occurred by preferential assembling of ceria nanorods along the longitudinal direction with the addition of AOT/toluene/water and H_2O_2/AOT/toluene/water microemulsions after a few weeks of aging. Such nanorods have an aspect ratio of 6 with a diameter of approximately 40 nm. In addition, according to the TEM analysis, it was proposed that the abrupt change in surface-free energy in the micelle might form the cone-shaped portions at both ends of the nanorods. Sun et al. [38] synthesized CeO_2 nanowires, 30–120 nm in diameter, by a precipitation method combined with thermostatic treatment using AOT as a template. Yada et al. [37] prepared different types of 1D nanowire structures with the presence of different-order alcohol and AOT as anions at 700°C or above. In the presence of AOT, adding lower-order alcohol such as alkyl or butyl alcohol and higher-order alcohol (octyl or dodecyl alcohol) only produced nanowire and the nanoring shape nanowire (diameter of ~280 nm and width of ~80 nm), respectively.

Lundberg et al. [52] prepared the mesoporous cerium dioxide flakes by using a copolymer surfactant (Pluronics 123) at ambient conditions in alcohol as a solvent. The material was produced via a direct calcination step, without the necessity of a gelling stage. According to the small angle X-ray scattering (SAXS) analysis, they observed that in the pluronic-ethanol mixture the surfactants were in a random coil state with no short-range or long-range order between them and combined with the cerium chloride precursor before the formation of pure CeO_2 mesoporous flakes. Son et al. [53] synthesized the ceria nanocubes through the reverse micelle method as the presence of aqueous solution of poly(oxyethylene) nonylphenyl ether (Igepal CO-520), cyclohexane, and hydrazine hydrate as a reducing agent. In a typical procedure, Gu et al. [27] successfully synthesized mesoporous ceria nanofibers, nanobelts, and rodlike nanoparticles using a reverse micelle method. They synthesized the mesoporous ceria nanofibers at the lower aging temperature at 30°C with a diameter of 50–200 nm and length of more than 50 μm with the presence of nonionic surfactant Triton X-100. On the other hand, nanobelts materials with the length of a few tens of μm, widths ranging from 0.5 to 5 μm, and the thicknesses ranging from 20 to 100 nm have been prepared at the slightly higher aging temperature at 40°C and constant time of 48 h, where BET surface area and pore volume of the nanobelts (114.9 m^2g^{-1} and 0.1470 cm^3g^{-1}, resp.) are about twice as high as those of the nanofibers (54.41 m^2g^{-1} and 0.09051 cm^3g^{-1}, resp.). In the presence of hexadecylamine and aqueous ethanol, solution may form hexagonal type comet structure. On the other hand, the presence of hexadecylamine and aqueous toluene solution can provide ceria nanocubic structure at 180°C for 24 h [54]. Bouchara et al. [55] investigated the coral-like, helical, or macroporous sieve morphologies with the presence of poly-g-benzyl-L-glutamate (PBLG) of organically functionalised CeO_2 crystalline nanoparticles. As an increase of the molar ratio s = nanoparticles/PBLG, phenyl-functionalized nanoparticles lead to the formation of coral-like structure ($s = 15$), helical ($10 < s < 60$), and macroporous where $s > 60$, respectively. Zhang et al. [56] formed the three-dimensional inverse opal type mesoporous structure by the presence of poly(methyl methacrylate) (PMMA) in cerous nitrates solution ($Ce(NO_3)_3 \cdot 6H_2O$) with alcohol (0.5 $molL^{-1}$), after drying and calcination at 350 to 800°C temperature. Similarly, Chen et al. [6] reported that novel ceria hollow nanocubes were synthesized through a solvothermal method using peroxyacetic acid (PAA) in anhydrous ethanol for 9 h at 160°C. Crystal growth of ceria hollow nanocubes was obtained through Oswald ripening method. It is observed that the prepared CeO_2 hollow nanocubes exhibit a higher catalytic activity toward CO oxidation. Andreescu et al. [57] investigated that thermal calcination process in the presence of air converts the initial precipitate amorphous spherical particles that consist of a complex mixture of ceria, ceria hydrate, cerium hydroxide, cerium glycolate complex, and residual propylene glycol, PG, to crystalline ceria. Similarly, the formation of monodispersed ceria particles was favored when polyethylene glycols (PEGs) of higher molecular weight were used [57–59]. Amino acid surfactant such as L-asparagine in the presence of $KBrO_3$ acts as OH provider and is followed by oxidizer to form hollow ceria sphere with a mean diameter of 1.5 μm and as shell thickness of 90 nm [60]. On the other hand, preparation of ceria aerogel is a novel technique to obtain higher-surface area (>200 m^2g^{-1}) for further water gas shift reaction, electrical conductivity analysis, and oxidation of propane application [61–63]. Recently, Gasser-Ramirez and coworkers synthesized the ceria aerogel in the presence of aqueous solution of 2-methoxyethanol and cerium(IV) methoxyethoxide through hydrolysis reaction [63].

3.2. Hard Template Techniques. Generally, the tubular structure itself may consist of higher thermal, chemical, and structural stability [50, 64–67]. Various preparation conditions have been employed to synthesize 1D Ce-NT materials, such as the use of different surfactants and templates, ultrasound treatment, hydrothermal method with different temperatures, aging effect, and acidic treatment. The template synthesis method is an effective way for preparation of the nanomaterials in the presence of polymeric filtration membrane and similar materials [50, 64–67]. Carbon nanotube (CNT) as a template plays a significant role in the formation of 1D ceria nanostructures. It was reported that the surface of the template was covered with ceria nanomaterials and possesses Ce-NT in the presence of pyridine. However, a homogeneous and continuous layer of ceria nanoparticles on CNTs is important for the formation

of Ce-NT. It should be noted that it is impossible to fabricate Ce-NT if the pyridine is replaced by DMF [68]. In addition, higher-temperature treatment was carried out for the removal of the templates [66–70]. The CNTs were refluxed in a mixture of concentrated KOH and NaOH at 450°C and that could be coated with CeO_2 for the formation of 1D nanotubular structures [69, 70]. The formation of Ce-NT is assisted with different methods just like ultrasonication, facile solvothermal method, and boiling reflux of ethylene glycol [66, 67, 71–74]. The preparation of Ce-NT is composed of several tiny interconnected nanocrystallites of about 10 nm in size. The pretreatment of CNTs and calcination temperature have been considered as crucial factors for determining the formation of Ce-NT. Metal ion doping is a promising technique to control the properties of material. Doping of metallic ion on the nanomaterials can influence the surface morphology, nanocrystal shape, and growth in solution. Laha and Ryoo [75] prepared the mesoporous cerium using the hexagonal p6mm and cubic Ia3d symmetries of the silica templates. Later on, Shen et al. [76] used the similar types of ordered mesoporous silica KIT-6 as a hard template for the formation of mesoporous ceria and doped CuO structure by wet impregnation technique. Hydrothermal method is a significant approach to synthesize the hollow ceria microspheres with around 70–100 nm shell thickness. On the other hand, polystyrene latex spheres as the template can be an influence on the formation of hollow ceria nanospheres in the two-step procedure [77, 78]. Fuentes et al. [64] obtained the mixed Zr-Ce-NT oxide in the presence of polycarbonate film through the microwave radiation at 800 W. The ordered CeO_2 nanowire arrays embedded in anodic alumina membranes (AAM) fabrication are also a novel technique. La et al. [28] and Wu et al. [79] fabricated CeO_2 nanowires with a diameter of 60–70 nm by using AAM as templates. As it showed in Figure 2, anions and cations are conversely migrated into the hexagonally ordered nanochannels of the AAM and are reacted inside the channels to form 1D nanostructures.

3.3. Nontemplate Techniques. The solvent composition and the cerium source precursor are of importance in the final product morphology [14–18]. The reaction temperature, concentration of the cerium precursor, and reaction time have a significant influence on the yield of CeO_2 nanorods [14]. Tang and coworkers [16] successfully obtained needle-shaped nanostructures at an environment with a higher amount of oxidizing agent and a higher concentration of the precursor. The surface area of the 1D cerium oxide was increased significantly with the calcination, attributable to the higher-temperature treatment initiating the crystallization into the nanostructures. Urea has a significant effect for the formation of one-dimensional nanostructure [80, 81]. In the presence of urea, Hirano and Kato [81] showed that the angular nanocrystalline ceria with a cubic fluorite structure were hydrothermally synthesized in the presence of three different types of cerium source cerium(III) chloride ($CeCl_3 \cdot 7H_2O$), and cerium(III) sulfate ($Ce_2(SO_4)_3 \cdot 8H_2O$), cerium(III) nitrate (Ce $(NO_3)_3 \cdot 6H_2O$). Later on, Wang and Lu [82] significantly investigated the concentration effect of urea for the formation of $CeOHCO_3$ at 160°C. At the lower urea concentration (0.05 M), a small amount of ceria with angular $CeOHCO_3$ is found with lower pH value from the unused urea solution. After an increase of the urea solution concentration from 0.1 to 1 M, the morphology of the $CeOHCO_3$ changes to rhomboidal platelets to prismatic shape with simultaneously increasing the pH value from the unused urea solution. They further explained that deprotonation of hydrated metal ions is accelerated at elevated temperatures. Once protons are released into the solution, the pH value of the solution will be lowered after the hydrothermal reaction, but at the increasing of urea concentration, a large amount of carbonate and hydroxyl ion is dissociated onto the solution to increase the pH [82]. In addition, phase transformation from orthorhombic $CeOHCO_3$ to cubic ceria takes place at the calcination temperature 500°C. Similar calcination temperature, in the presence of 2 mL of 0.01 M $Ce(NO_3)_3$ in 40 mL of distilled water and 1.0 g of urea at 150°C for 12 h in the hydrothermal process, can form spindle-type ceria structure [80]. Spindle ceria nanomaterial is effective for optoelectrical application. Sequentially, morphology of metallic-doped ceria one-dimensional structure has the significant effect in optoelectrical and chemical conversion reaction. Huang et al. [20] synthesized Au/CeO_2 nanorods with the wet chemical reducing system in the presence of $NaBH_4$ solution, as a reducing agent. They also observed that hydrothermal temperatures influenced the nucleation and crystal growth of the CeO_2 nanorod. Morphological transformation of the nanorod was not completed with hydrothermal temperatures below 150°C at 5 or 10 M KOH solution. Consequently, higher-alkaline concentration provides thicker nanorod structures. Therefore, it would be considered that higher-alkaline concentration is involved in increasing the width of the nanostructures rather than the nucleation of length of the samples. Similar to this approach, it was also confirmed for the formation of different shape of cerium oxide 1D nanostructures with the presence of different concentrations of alkali [21]. At lower precipitation concentrations, the shape of nanopolyhedra, and at the higher concentrations, a mixture of rods and polyhedral shapes were provided, respectively. On the other hand, the precipitant mainly formed the cubic and rod-shaped structure at higher temperature and higher concentrations, respectively. Zhou et al. [19] obtained the CeO_2 nanorods of 15–30 nm in diameter and lengths of up to tens of micrometers by a precipitation method combined with the hydrothermal treatment with the presence of alkali solution. Ge et al. [83] successfully used the emulsion liquid membrane system to synthesize CeO_2 sponge-like rods with diameters of 170–810 nm and lengths of 5–10 μm, which were successfully fabricated through a route of liquid emulsion membrane followed by heat treatment. Recently, Macedo et al. [84] developed the ceria nanorod in the presence of higher concentration of NaOH (12 M) and in the presence of $Ce_2(SO_4)_3 \cdot 9H_2O$ at 135°C for 15 h. They observed that pretreatment of CeNR with H_2O_2 or *t*-BuOOH prior to reaction of PhEt with *t*-BuOOH leads to faster reaction than CeNR. He et al. [85] investigated

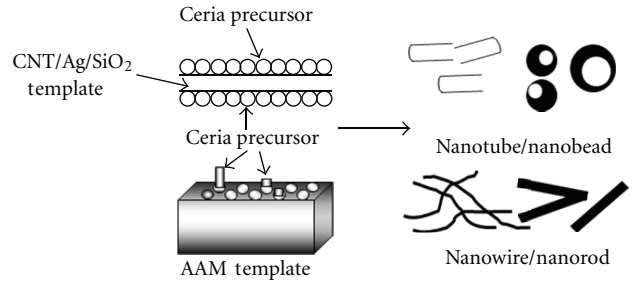

Figure 2: Schematic illustration for the formation of one-dimensional nanostructures using hard template methods.

the correlations between the shape and size of ceria nanostructure and the mechanical performance of composite with the presence of epoxy resin. They found that epoxy resins made with high-aspect-ratio ceria nanorods show the four-times-higher-impact strength up to 17.27 kJ m^{-2}, where size and shape are influenced to enhance the strength of composite materials. The one-step synthesis of CeO_2 nanorods is still a challenge. In this case, ultrasonication methods have been successfully used to prepare nanorods. In the previous reports, the synthesis methods of CeO_2 nanorods were relatively complicated and always needed high-temperature, high-pressure, or long-time treatments [22–24]. In addition, Qi et al. [22] synthesized the thicker CeO_2 microrod (200–250 nm in diameter and 600–1200 nm in length) by an ultrasonication process than surfactant-assisted hydrothermal method.

Recently, Gao et al. [25] approached the microwave-hydrothermal method for the facile, rapid synthesis of higher yields of 1D CeO_2 with average sizes of ~1.6 nm to ~20 nm. Compared with a conventional hydrothermal method, the microwave-assisted hydrothermal method shows advantages of rapidity, convenience, and cost effectiveness and could be potentially extended to the synthesis of other nanoparticles and nanorods. On the other hand, Tang et al. [16] simply used the hydrothermal method to achieve nanowires with nonsurfactant-assisted method. They observed that the presence of acidic precipitant H_2O_2 with 0.1 M $Ce(NO_3)_3$ produces the nanowire and nanocubes, whereas a lower concentration of the precursor (0.05 M $Ce(NO_3)_3$) formed only nanowire diameters of 20–70 nm and lengths up to 40 μm in the hydrothermal process at 250°C for 3 h. Furthermore, aggregated nanoneedles have been formed as the absence of oxidizing agent H_2O_2. Nanowires were structurally uniform and single crystalline. The interplane distance in this research was obtained as 0.28 nm, corresponding to the separation between the (200) lattice planes of cubic CeO_2. It is evident that complete and controlled conversion of CeO_2 nanostructures through templates is not readily achievable. Additionally, fabrication and removal of the template have been achieved as very troublesome techniques for the Ce-NT synthesis process. Therefore, the formation of 1D nanotubes with the absence of templates has been attractive owing to simple, quick, and economical considerations. On an important low-cost basis, Miao et al. [86] developed the procedure of ultrasound irradiations, in order to prepare Ce-NT from ceria nanoparticles at room temperature. In addition, Dos Santos et al. [87] explained that the calcined temperature readily affected the crystallinity and morphology of the CeO_2 nanostructure. Thus, the development of a facile and controllable formation of Ce-NT with proper crystalline structure is of great significance.

One of the most notable characterizations of the fluorite Ce-NT has been recently developed by a hydrothermal method. Han et al. [88] synthesized the yellowish CeO_{2-x} nanotubes, nanowire, and nanoparticles in two steps. At the beginning, the samples were prepared at 100°C in the presence of 7 mL of 5% ammonia hydroxide solution and then aged at 0°C for 45 days. This procedure is time consuming. Tang et al. [89] proposed the lamellar rolling of the $Ce(OH)_3$ crystal nanotubes through the alkali treatment of the trivalent ceria salt $CeCl_3$ at 120°C under an oxygen-free environment with the hydrothermal method. They observed that 1D Ce-NT was obtained from the annealing of $Ce(OH)_3$ crystal nanotubes in the reducing atmosphere. Pan and coworkers [32] observe that cerium oxide nanorods are easily obtained under a higher concentration of alkali treatment (10–15 M) at room temperature to up to 100°C temperature with the presence of $Ce(NO_3)_3$ as a precursor. When $Ce(NO_3)_3$ is replaced by $(NH_4)_2Ce(NO_3)_6$, CeO_2 nanorods are not obtained. According to the LSW theory and analysis, nitrate from $(NH_4)_2Ce(NO_3)_6$ has noncomplexing characteristics for the formation of one-dimensional ceria nanostructure. In addition, they explained that accumulation of the Ce^{3+} ion for 72 h on the cerium oxide nanorod surface would provide Ce-NT in the hydrothermal condition around 100°C. As well, at increasing temperature, the deposition of Ce^{3+} ion occurred at the tip of the nanorod and formed the nanowire and subsequently nanocubes. It was also shown that a larger surface area was achieved by the lower-temperature nanorod preparation. However, this method is an effective way for the preparation of Ce-NT in the case of the template-free controlled conversion system.

Chen et al. [90] synthesized Ce-NT with a simple solid liquid interface reaction route in the absence of any surfactants by employing $Ce(OH)CO_3$ nanorods as precursors. Recently, Wang et al. [91] synthesized the nanospheres, and nanowires, and nanorods can be obtained through a surfactant and template-free solution simply by varying the anionic composition or the type of counter ion, such as chloride, nitrate, and phosphate in solution before the hydrothermal

treatment. As a synthesis of hydrothermal method, Zhou et al. [92] converted CeO_2 nanorods into nanotubes in an acidic treatment like H_2O_2 solution assisted by ultrasonication. The converted Ce-NT has a higher reducible property, which was due to the higher activity of CeO_2 surface (100) than that of common surface (111) [92, 93]. In addition, CeO_2 nanorods consisted of Ce^{4+} as a surface material and Ce^{3+} as inside [92]. On the other side, Han et al. [88] obtained the opposite phenomenon, since the fraction of Ce^{3+} is significantly larger than that of CeO_{2-x} nanoparticles with the same diameter. Thus, Ce^{3+} ions remained on the surface of the 1D Ce-NT. Chen and coworkers [94], through the Kirkendall effect, obtained 1D Ce-NT in which Zr^{4+} ions may act as the catalyst to promote the diffusion rate of Ce^{3+}/Ce^{4+} ions inside the nanorod as shown in Figure 3. According to a partial oxidation of Ce^{3+} ions and differential rate of diffusion between Ce^{4+} and Ce^{3+} ions inside the material, the metal hydroxide nanorods gradually decompose to form $Zr_xCe_{1-x}O_2$ nanotubes. Chen et al. [65] studied three different ways for the formation of ceria nanotube on the basis of the Kirkendall effect (denoted as K-type), template (T-type), and lamellar rolling (L-type). The K-type Ce-NT had been prepared by congregating Kirkendall voids, and subsequent calcinations were acquired in the presence of air at 600°C for 4 h. In addition, T-type and L-type nanotubes had been obtained without any calcination. Precipitant and the reaction temperature are implicated in the formation of the K-type ceria nanotube. Furthermore, Martin et al. [95] used the atomistic simulation techniques based on the Born model of solids to observe multilayer Ce-NT with a wall thickness of 5.5 nm and a lumen diameter of 4.8 nm. Besides, the 1D ceria nanostructure was achieved with the electrochemically synthesized route through change of the electric field, strength, and direction by Fu et al. [96]. They acquired the morphologies of ceria nanomaterials from nanoparticles and nanorods to nanowire by simply changing the potential direction and time of anodic oxidation. Tuning the ammonium acetate concentration through the precipitation method, Bugayeva and Robinson [97] controlled the particle size, shape, and agglomeration of the 1D nanowire. The hydrated CeO_2 nanowires as thin as 5 nm in diameter and nanoneedles with various aspect ratios were obtained via a chemical precipitation technique in the presence of ammonium acetate. However, Tang et al. [16] proposed and explained that the concentration of an oxidant such as H_2O_2 would significantly affect to impose the cone type or needle-like phenomenon in the 1D cerium structure.

4. Applications

In recent years, oxidation catalysts are receiving considerable attention because of their potential role in the environmentally important fuel cell technologies. As an important component in catalysts, ceria promote high oxygen storage capacity (OSC) and high oxygen ion conductivity. Several morphological structures of CeO_2 such as nanorod, nanosponge single or multiwall, hollow structure, mesoporous, spindle have been investigated widely for the selective oxidation of mainly carbon monoxide, nitrogen oxides, sulfur oxide, and so on, due to OSC of ceria.

4.1. Advantage of 1D Structured Cerium Oxide for Carbon-Monoxide Oxidation Reaction. The catalytic performance of the 1D CeO_2 nanomaterials is affected with the structure and surface area as shown in Table 1. As well, surface area, structural defects, and oxygen vacancy have a positive effect on CO oxidation [15]. Zhang et al. [2] have compared the two different kinds of 1D nanomaterials to exhibit the CO oxidation, where they derived that CeO_2 single/multiwall hollow microspheres may provide CO total conversion at 230°C and for bulk CeO_2 is 500°C, respectively. Hollow microspheres afford more available oxygen and oxygen deficiency for CO oxidation [1, 2, 99]. In addition, high catalytic activity on CO oxidation was obtained for CeO_2 single/multiwall hollow microspheres and consisted of similar activity at 240°C for T_{100} in the second and the third runs, which revealed its excellent thermal stability and recycling performance [2]. Similar tendency of the CO oxidation was followed for the hollow nanobeads and hollow nanocubes [6, 99]. CNT templates in the CeO_2 hollow nanobeads may be formed by $CeO_{2-x}C$ and thus increase the catalytic activity [99]. According to Chen et al. [6], the CO conversion of CeO_2 hollow nanocubes is 56% and almost 3.5 times higher than that of the CeO_2 powder at 270°C. They explained that the interconnected hollow structure enables better contact with the gas molecule owing to the existence of interior spaces: penetrable shell and that influenced to exhibit effective performance. The stability and recycling performance of CeO_2 catalyst are important factors for the practical applications. According to TEM analyses, they demonstrated that the hollow structure has not been collapsed at a high temperature (300°C), and the catalytic operation has been conducted after the reactor cooled down to room temperature, which demonstrated its excellent stability and recycling performance [1, 6]. On the other hand, the overall catalytic activity and the BET specific surface area are affected with the preparation method of the catalyst [18, 100]. Masui et al. [100] reported that the CeO_2/Al_2O_3 catalyst prepared by the microemulsion method shows higher activity for carbon monoxide oxidation although CeO_2/Al_2O_3 catalyst surface area is as low as that prepared by the coprecipitation method. Pan and coworkers [18] have explained that nanomaterials consist with similar BET-specific area are greatly influenced by the crystal surface to represent the catalytic activity. They also observed that CeO_2 nanorods, nanoplate, and nanotubes are exhibited with higher BET surface area: 52.5, 37.2, and 80.1 m^2g^{-1}, respectively, in addition, nanoplates consisted of higher crystal surface (100) and that contributes to create enormous oxygen vacancies and thus favors the higher catalytic performance.

Most recently, Zhang et al. [11, 13, 101, 102] synthesized various ceria micro/nanostructures such as spheres, spindles, columns, spheres, and rods and then investigated the catalytic activity in the oxidation of carbon monoxide. Regarding the several types of nanostructures such as spindle, rod the effect of carbon monoxide oxidization of CeO_2

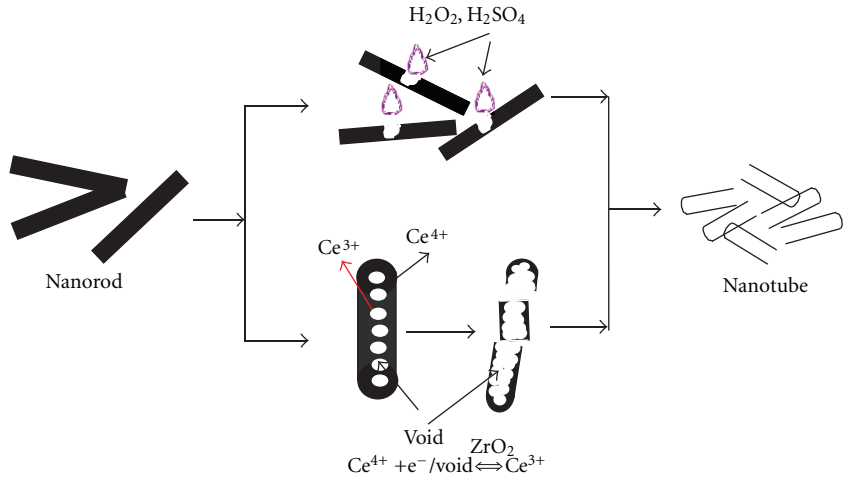

Figure 3: Schematic illustration of Kirkendall effect for the formation of one-dimensional structures.

Table 1: Carbon-monoxide oxidation onto several ceria nanostructures.

Sample	T_{50} (°C)	T_{100} (°C)	BET (m^2g^{-1})	Reference
Bulk Ceria	300–435	500	5–15	[9, 67]
Nanoparticle	220–305	300–380	30–115	[15, 19, 32, 51, 67]
Nanorod	190–290	205–345	50–128	[15, 18, 19, 32]
Nanotube	223–265	230–325	44–98	[2, 18, 32, 67]
Nanowire	245	N.A.	79.8	[32]
Nanocube/bead	240–315	300	87–115	[2, 6, 32, 51, 76]
Metal/CeO_2 nanostructure	110–270	130–320	70–165	[9, 20, 76, 103]

"N.A." denotes "not available".

was revealed by Ho et al. [15]. The spindle-like sample shows the highest CO conversion rate 0.861 μmol $g^{-1}s^{-1}$, which is almost 4.5 times higher than CeO_2 particles (as referred to), 0.189 μmol $g^{-1}s^{-1}$. According to XRD analysis, they observed that the order of the lattice cell volume was strongly related to the degree of Ce^{4+} reduction and the extent of oxygen vacancy. Interestingly, the surface area and pore volume of the samples were significantly increased after calcinations and affected the CO oxidation. The same result for the effects of surface area was also demonstrated for the ceria nanorod and sponge nanorod [19, 83]. Zhou et al. [19] have attained that CeO_2 nanorods are three times more active than CeO_2 nanoparticles for CO oxidation and found that the T_{100} (the temperature at which the CO conversion is 100%) for the CeO_2 nanorods and CeO_2 nanoparticles catalysts approachs to 275 and 300°C, respectively. In addition, using CeO_2 sponge-like rods as a catalyst, the T_{100} is only 205°C, which shows that catalytic property of CeO_2 sponge-like rods has an advantage over that of CeO_2 nanorods and CeO_2 nanoparticles [83]. The sponge nanorod may provide a larger percentage of atoms onto the surface and would create structural defects and generate pronounced oxygen vacancies than nanorod or nanoparticles [19, 64, 83]. Similar tendency is also observed for the case of ceria nanotube [67], therefore it could provide the three times higher catalytical activity than bulk ceria and ceria nanoparticle.

Recently, Pan et al. [32] explained that 1D ceria nanorods synthesized at a low temperature with enough aging time possess a large BET-specific area and thus provide a perfect crystalline form and have a high performance for CO oxidation. The physical and chemical properties of ceria could be tuned by doping with different metals to obtain low-temperature reducibility (Au, Cu, Pr, and Sn). Metallic doping with tetravalent cations, (such as Zr and Hf) onto the ceria nanostructures, may enhance the OSC and consequently archive high ionic conductivities with trivalent cations (such as La, Sm, Gd, and Y) [8, 9, 103]. Sunder and Deevi [8] observed that the catalytic activity of the CO oxidation with Cu-CeO nanocomposite may significantly increase due to the addition of CuO. A similar research was also observed by Sun et al. [9]. They have seen that the quickly accelerated CO conversion starts below 120°C, and complete CO oxidation is achieved at about 220°C over the catalysts containing more than 10 wt% CuO onto the 3-D flower-type CeO_2 nanomaterials. The performance of the flowerlike CeO_2 microspheres loaded with 20 wt% CuO became worse, and 15 wt% CuO sample had the best catalytic activity for CO oxidation. It may be affected with higher content of the CuO or surface-volume ratio of the catalyst [8, 9]. However, Shen et al. [76] observed that up to 20% of molar ratio CuO loaded onto mesoporous ceria nanostructure has higher catalytic activity for CO oxidation.

The role of the support and the oxygen supply for the catalytic reaction remains controversial. Although it is accepted that factors, such as gold particle size, synthesis method, pretreatment conditions, and support, influence the reactivity of the supported gold catalysts the nature of the active sites and the reaction mechanism for CO oxidation are still subjects of debate. According to Raman spectroscopic analyses, Guzman et al. [103] indicated that nanocrystalline CeO_2 in the presence of gold catalyst, supplies reactive oxygen in the form of surface η^1 superoxide species and peroxide adspecies. The conventionally precipitated CeO_2 tends to stabilize $O_2{}^{\delta-}$ $(0 < \delta < 1)$ adspecies and molecular O_2 onto the surface. Thus, both cationic and metallic gold are attributed in nanocrystalline CeO_2 to accelerate CO oxidation at low temperatures. The formation of the surface chemisorbed oxygen species can be facilitated by defects in the catalyst structure. Therefore, Sun et al. [9] demonstrated the 2.77 wt%, of Au-loaded flower-like CeO_2 microsphere catalysts highly active with CO gas conversion into CO_2 above 80% at room temperature, and T_{100} is observed at 130°C. On the other hand, around 81% CO conversion is achieved at 220°C for Au/CeO_2 nanorod as a catalyst, while only 20−22% CO conversion is obtained at the same temperature for pure CeO_2 nanorods and nanoparticles as a catalyst [20]. The catalytic activities of Au/CeO_2 flower, nanorods, and nanoparticles are much higher than those of pure CeO_2 nanorods and nanoparticles, consequently [9, 20].

4.2. Advantage of One-Dimensional Cerium Oxide for CH_3OH/SRM Reaction. Several researchers to optimize the catalysts for a carbon monoxide oxidation reaction have investigated the effect of different structure of ceria nanomaterials and the impact of metal loading. In addition, the ceria and doped ceria nanomaterial would also be used for the SRM reaction, whereas the preparation procedure, size, and shape are effectively influenced by the SRM reaction. Several synthesis techniques have been applied to obtain the different structure of ceria [98, 104–107]. Porosity and surface structure of the ceria nanomaterials facilitate to obtain the utmost performance for the catalytic reaction. These properties can also be changed by the concentration differences for presols and the treatment procedures of the drying and calcinations temperatures. There are three process alternatives to produce hydrogen through the conversion of methanol: (1) decomposition, (2) partial oxidation and (3) steam reforming. Different reactions were involved in a reactor with different enthalpies to achieve hydrogen-rich gas from methanol at standard condition [98, 104–106]. The decomposition reaction is the simplest process from a chemical point of view as solely methanol is used as feedstock as shown below [98, 104–107]:

$$CH_3OH \longrightarrow 2H_2 + CO \quad \Delta Hr = 92\,kJmol^{-1}. \tag{3}$$

However, the reaction is strongly endothermic, which means that it requires a lot of energy for operating. Furthermore, the decomposition yields product gas containing up to 67% of hydrogen and 33% of carbon monoxide. The high content of the CO clean-up system is regarded to be the most complicated part in the fuel cell system. Because of these drawbacks, the decomposition of methanol is found to be unsuitable for fuel cell applications. This shortcoming could be overcome with the CO oxidation through the promising catalyst ceria. In contrast to the decomposition reaction, partial oxidation is a fast and exothermic reaction as represented below:

$$CH_3OH + 0.5O_2 \longrightarrow 2H_2 + CO_2 \quad \Delta Hr = -192\,kJmol^{-1}. \tag{4}$$

Several studies on this reaction have been published in the last few years [104]. The advantage of this process with respect to the exothermic nature is that an additional energy supply for the reaction is not necessary. However, the exothermic behavior should be taken into account when designing the reactor. The fast increase of temperature in the reactor can form hot spots, which can cause the deactivation of the oxidation catalyst through sintering of the metal particles. The hydrogen concentration up to 67% in a product stream can be achieved when methanol is partially oxidized with pure oxygen in the feed. The oxygen required for the automobile application would most likely be supplied from air. Due to the high content of nitrogen in the air, this causes dilution of the product gas with nitrogen. As a result, the maximum theoretical hydrogen content in such a system is lowered to 41%. The decrease of the hydrogen content in the product stream influences strongly the performance of the electricity production in fuel cell [104]. The steam reforming of methanol (SRM) is known as a reverse reaction of methanol synthesis as follows:

$$CH_3OH + H_2O \longrightarrow 3H_2 + CO_2 \quad \Delta Hr = 49.4\,kJmol^{-1}. \tag{5}$$

SRM is considered to be the most favorable process of hydrogen production in comparison to the decomposition and partial oxidation of methanol. This is because of the ability to produce gas with high hydrogen concentration (75%) and high selectivity for carbon dioxide. SRM is an endothermic reaction. Another additional alternative to produce hydrogen from methanol is to combine the partial oxidation with the steam reforming. The advantage of this process is that heat requirement for the reaction can be supplied by the reaction itself (autothermal reaction). However, the concentration of hydrogen in gas product and methanol conversion is lower than that in the SRM [108]. Yi and coworkers found that small amount of gold-doped one-dimensional ceria nanomaterial was significantly more active and selective towards CO_2 at temperatures below 250°C [109]. Strong-bonded Au_n–O–Ce species are the active sites for the SRM reaction, and the apparent activation energies are not dependent on the shape of the ceria. The catalytic properties of these catalysts, such as activity, CO_2 selectivity, were studied by means of a fixed bed reactor. In order to evaluate the catalytic properties of the different-dimensional ceria and dope catalysts, a commercial ceria catalyst was used as a reference. A kinetic study for the synthesis of the different structure of the ceria nanomaterial is also performed in this

work. They pointed out that the 1% Au-ceria (rod) catalyst shows excellent activity for the water-gas shift reaction, comparable to Au-ceria nanopowders, including Au-ceria with a high surface area of 250 m^2g^{-1}, while the Au-ceria (cube) is inactive.

The SRM produces a relatively small amount of carbon monoxide at low temperatures whereas carbon monoxide is known to be very poisonous for Pt catalysts in a proton exchange membrane fuel cell (PEMFC) system [113]. In addition, autothermal reforming of the methanol (ATRM) process leads to produce a higher amount of hydrogen and consists with CO as a by-product which has the negative impact on PEMFC operation. Therefore, there is great interest in developing highly selective catalysts as follows:

$$2CH_3OH(g)+H_2O(g)+\frac{1}{2}O_2 = 2CO_2+5H_2 \quad \Delta H=-142.8\ \text{kJ mol}^{-1}. \tag{6}$$

The catalytic reaction for SRM and ATRM is generally based on copper or palladium, where Pd has consisted of higher thermal stability and the production of large content of CO with lower selectivity from methanol decomposition. On the other hand, Cu-based catalyst has consisted of low cost, higher reactivity, and selectivity [114, 115]. Copper catalyst is effectively dispersed in ZnO or ZnO/Al_2O_3 to generate mesoporosity, with high-surface area and good thermal stability, exhibited interesting catalytic activity in the CO preferential oxidation reaction. Thus, $CuO/ZnO-Al_2O_3$ is one of the most used catalysts for hydrogen generation by ATRM in a microchannel reactor [116, 117]. Cerium-promoted copper catalyst existed for the recovery of hydrogen from methanol with the optimization of carbon monoxide concentration [118]. Furthermore, ceria hindered Cu sintering in Cu/Al_2O_3 catalysts and increased thermal stability and catalytical reactivity [112]. According to our recent work in Figure 4 and Table 2 [98], we observe that ceria accompanied with the copper metal complexes formation is influenced by the catalytic activities on the ATRM reaction in the microchannel reactor to generate hydrogen for further application of a fuel cell system, where as-synthesized homogeneous sol was prepared by adding 20 g as-synthesized catalyst (CuO 40%, ZnO 50%, and Al_2O_3 10%) to form the catalyst slurry (S20) and combined with the CeO_2 sol (B) 1 to 10 wt.% of solid content, respectively. Ceria promote to reduce the poisonous carbon monoxide to carbon-dioxide. According to the XRD and XPS data analyses, we confirmed that catalyst content copper species strongly interact with CeO_2 to from Cu–O–Ce. Moreover, a hydrogen production rate of 2.16 Lh^{-1} is obtained, and the corresponding methanol conversion is 100% at 270°C for ceria sol washcoat catalysts. After the activation of the catalyst (S20-B2), methanol started to decompose, and the conversion was above 95% at 240°C. In addition, a higher temperature was required for higher methanol conversion but decreasing with the increase of feed flow rate and was related with the steam to carbon (methanol) ratio [107, 111, 119]. According to the Seo et al. [107], methanol conversion was achieved 90% at 260°C, and the feed flow rate was

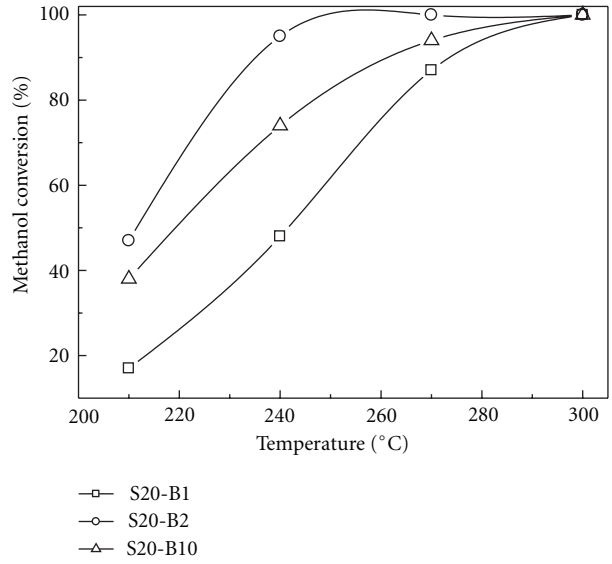

Figure 4: Methanol conversion of $Cu/ZnO-Al_2O_3$ catalyst with CeO_2 binder washcoats of (a) S20-B1, (b) S20-B2, and (c) S20-B10, respectively, for the steam reforming of methanol in a microreactor (steam/MeOH = 1.3; WHSV = 16.2 $g_{MeOH}\,h^{-1}\,g_{cat}{}^{-1}$; loading weight of washcoat catalyst = 20 mg/plate) [98].

0.2 $cm^3\,min^{-1}$. A hydrogen production rate of 2.16 Lh^{-1} was obtained at a feed rate of methanol liquid mixtures of 0.05–0.2 mL min^{-1} with a WHSV of 16.2 $g_{MeOH}\,h^{-1}\,g_{cat}{}^{-1}$. Moreover, the selectivity of hydrogen and carbon dioxide was high enough, and a typical dry gas composition of the present system was 73-74% H_2, 24-25% CO_2, and <0.1% CO gas products, respectively. Nevertheless, $T_r > 260 \pm 10$°C were also required in the cases to achieve high methanol conversion [112, 120–124]. The addition of ceria caused the synergistic effect to give the activity enhancement. However, methanol conversation was decreased to 95% at 270°C for S20-B10. Avgouropoulos and coworkers [110] studied the effect of methanol decomposition (MD), SRM, and ATRM reaction on the noble metal/ceria catalysts process. They observed that catalytic activity increases in the order of Rh < Pt < Pd/Ceria for all three processes, where H_2 and CO are the major products, while ethylene, ethane, and propylene are formed only over Rh/CeO_2 at $T \geq 270$°C with selectivities lower than 0.5%. The H_2 yield and CO selectivity increase with the temperature. Due to the morphology and porosity, BET surface area significantly affects the catalytic activity. This confirms that ceria-based catalyst is suitable for ATRM reaction with the integrated PEMFC application on energy generation.

5. Conclusions

In this paper, we have shown how one-dimensional ceria nanomaterial synthesizes on the template and nontemplate methods. The key issue for large scale of one-dimensional ceria nanostructure for further catalytical applications is the development of the synthesis methods that implies for

Table 2: Comparison of the MD/SRM/ATRM performances over different metal-doped CeO_2 catalysts in literatures.

Catalyst	S/C[a]	WHSV[b] (GHSV)[b]	S_{CO}^{c} (%)	T^{d} (°C)	Reference
Pt/CeO_2[e]	N.A.	(42,000)	1.41	270 (100)	[110]
Pd/CeO_2[e]	N.A.	(42,000)	0.589	270 (100)	[110]
Rh/CeO_2[e]	N.A.	(42,000)	44.6	270 (100)	[110]
Pt/CeO_2[f]	1.5	(42,000)	0.86	270 (100)	[110]
Pd/CeO_2[f]	1.5	(42,000)	20.46	250 (100)	[110]
Rh/CeO_2[f]	1.5	(42,000)	19.89	270 (100)	[110]
Ceria (nanorods)[f]	1.3	(42,000)	N.A.	450 (95)	[109, 111]
Ceria (nanocubes)[f]	1.3	(42,000)	N.A.	500 (95)	[109, 111]
1% Au-ceria (rod)[f]	1.3	(42,000)	N.A.	300 (95)	[109, 111]
1% Au-ceria (cube)[f]	1.3	(42,000)	N.A.	380 (95)	[109, 111]
Pt/CeO_2[g]	1.5	(42,000)	0.729	270 (100)	[110]
Pd/CeO_2[g]	1.5	(42,000)	22.27	250 (100)	[110]
Rh/CeO_2[g]	1.5	(42,000)	2.52	270 (100)	[110]
$Cu_{40}Zn_{50}Al_{10}$-CeO_2[g]	1.3	16.2	0.58	300 (95)	[98, 105]
$Cu_{40}Zn_{50}Al_{10}$-CeO_2[g]	1.3	16.2	0.40	240 (95)	[98, 105]
$Cu_{40}Zn_{50}Al_{10}$-CeO_2[g]	1.3	16.2	0.35	270 (95)	[98, 105]
$Cu_{50}Zn_{33}Al_8$-Al_2O_3[g]	1.1	54.0	2.90	260 (99)	[98, 105]
$Cu_{50}Zn_{33}Al_8$-Al_2O_3[g]	1.5	14.8	1.10	270 (80)	[98, 105]
$Cu_{65}Zn_{28}Ce_7$-Al_2O_3[g]	1.3	8.3	2.05	292 (97)	[98, 105, 112]
$Cu_{48}Zn_{48}Ce_4$-Al_2O_3[g]	1.3	8.3	1.30	292 (98)	[98, 105, 112]
$Cu_{38}Zn_{58}Ce_4$-Al_2O_3[g]	1.3	8.3	1.60	292 (91)	[98, 105, 112]
$Cu_{48}Zn_{48}Ce_4$-Al_2O_3[g]	1.3	8.3	2.10	292 (88)	[98, 105, 112]

S/C[a]: steam-to-carbon ratio; WHSV[b]: weight hourly space velocity in mass methanol per time and mass of catalyst ($g_{MeOH}\ h^{-1}\ g_{cat}^{-1}$); (GHSV)[b]: (gas hourly space velocity at NTP (h^{-1})); S_{CO}[c] (%): CO selectivities; T[d] (°C): temperatures required for conversion of methanol at different percentage; [e]: methanol decomposition; [f]: steam reforming reaction; [g]: autothermal reforming of methanol; N.A.: not available.

the production of one-dimensional structure with large-surface areas. Current investigation through this work directed towards the application of ceria nanomaterials readily involved the size, shape, and structure, which are likely to display higher-catalytic phenomenon.

Acknowledgment

The financial supports of the National Science Council (Contract no. NSC-97-2221-E-155-005) of Taiwan are gratefully acknowledged.

References

[1] S. S. Deshmukh, M. Zhang, V. I. Kovalchuk, and J. L. D'Itri, "Effect of SO_2 on CO and C_3H_6 oxidation over CeO_2 and $Ce_{0.75}Zr_{0.25}O_2$," *Applied Catalysis B*, vol. 45, no. 2, pp. 135–145, 2003.

[2] Y. Zhang, T. Cheng, Q. Hu, Z. Fang, and K. Han, "Study of the preparation and properties of CeO_2 single/multiwall hollow microspheres," *Journal of Materials Research*, vol. 22, no. 6, pp. 1472–1478, 2007.

[3] M. Y. Cui, J. X. He, N. P. Lu et al., "Morphology and size control of cerium carbonate hydroxide and ceria micro/nanostructures by hydrothermal technology," *Materials Chemistry and Physics*, vol. 121, no. 1-2, pp. 314–319, 2010.

[4] Z. Sun, H. Zhang, G. An, G. Yang, and Z. Liu, "Supercritical CO_2-facilitating large-scale synthesis of CeO_2 nanowires and their application for solvent-free selective hydrogenation of nitroarenes," *Journal of Materials Chemistry*, vol. 20, no. 10, pp. 1947–1952, 2010.

[5] Z. Guo, F. Jian, and F. Du, "A simple method to controlled synthesis of CeO_2 hollow microspheres," *Scripta Materialia*, vol. 61, no. 1, pp. 48–51, 2009.

[6] G. Chen, C. Xu, X. Song, S. Xu, Y. Ding, and S. Sun, "Template-free synthesis of single-crystalline-like CeO_2 hollow nanocubes," *Crystal Growth and Design*, vol. 8, no. 12, pp. 4449–4453, 2008.

[7] P. Fornasiero, R. Dimonte, G. R. Rao et al., "Rh-loaded CeO_2-ZrO_2 solid-solutions as highly efficient oxygen exchangers: dependence of the reduction behavior and the oxygen storage capacity on the structural-properties," *Journal of Catalysis*, vol. 151, no. 1, pp. 168–177, 1995.

[8] R. S. Sundar and S. Deevi, "CO oxidation activity of Cu-CeO_2 nano-composite catalysts prepared by laser vaporization and controlled condensation," *Journal of Nanoparticle Research*, vol. 8, no. 3-4, pp. 497–509, 2006.

[9] C. Sun, H. Li, and L. Chen, "Study of flowerlike CeO_2 microspheres used as catalyst supports for CO oxidation reaction," *Journal of Physics and Chemistry of Solids*, vol. 68, no. 9, pp. 1785–1790, 2007.

[10] H. Mai, D. Zhang, L. Shi, T. Yan, and H. Li, "Highly active $Ce_{1-x}Cu_xO_2$ nanocomposite catalysts for the low

temperature oxidation of CO," *Applied Surface Science*, vol. 257, no. 17, pp. 7551–7559, 2011.

[11] D. Zhang, H. Mai, L. Huang, and L. Shi, "Pyridine-thermal synthesis and high catalytic activity of CeO_2/CuO/CNT nanocomposites," *Applied Surface Science*, vol. 256, no. 22, pp. 6795–6800, 2010.

[12] K. S. Lin and S. Chowdhury, "Synthesis, characterization, and application of 1-D cerium oxide nanomaterials: a review," *International Journal of Molecular Sciences*, vol. 11, no. 9, pp. 3226–3251, 2010.

[13] F. Niu, D. Zhang, L. Shi et al., "Facile synthesis, characterization and low-temperature catalytic performance of Au/CeO_2 nanorods," *Materials Letters*, vol. 63, no. 24-25, pp. 2132–2135, 2009.

[14] C. Sun, H. Li, H. Zhang, Z. Wang, and L. Chen, "Controlled synthesis of CeO_2 nanorods by a solvothermal method," *Nanotechnology*, vol. 16, no. 9, pp. 1454–1463, 2005.

[15] C. Ho, J. C. Yu, T. Kwong, A. C. Mak, and S. Lai, "Morphology-controllable synthesis of mesoporous CeO_2 nano- and microstructures," *Chemistry of Materials*, vol. 17, no. 17, pp. 4514–4522, 2005.

[16] B. Tang, L. Zhuo, J. Ge, G. Wang, Z. Shi, and J. Niu, "A surfactant-free route to single-crystalline CeO_2 nanowires," *Chemical Communications*, no. 28, pp. 3565–3567, 2005.

[17] A. Vantomme, Z. Y. Yuan, G. Du, and B. L. Su, "Surfactant-assisted large-scale preparation of crystalline CeO_2 nanorods," *Langmuir*, vol. 21, no. 3, pp. 1132–1135, 2005.

[18] C. Pan, D. Zhang, and L. Shi, "CTAB assisted hydrothermal synthesis, controlled conversion and CO oxidation properties of CeO_2 nanoplates, nanotubes, and nanorods," *Journal of Solid State Chemistry*, vol. 181, no. 6, pp. 1298–1306, 2008.

[19] K. Zhou, X. Wang, X. Sun, Q. Peng, and Y. Li, "Enhanced catalytic activity of ceria nanorods from well-defined reactive crystal planes," *Journal of Catalysis*, vol. 229, no. 1, pp. 206–212, 2005.

[20] P. X. Huang, F. Wu, B. L. Zhu et al., "CeO_2 nanorods and gold nanocrystals supported on CeO_2 nanorods as catalyst," *Journal of Physical Chemistry B*, vol. 109, no. 41, pp. 19169–19174, 2005.

[21] H. X. Mai, L. D. Sun, Y. W. Zhang et al., "Shape-selective synthesis and oxygen storage behavior of ceria nanopolyhedra, nanorods, and nanocubes," *Journal of Physical Chemistry B*, vol. 109, no. 51, pp. 24380–24385, 2005.

[22] R. J. Qi, Y. J. Zhu, G. F. Cheng, and Y. H. Huang, "Sonochemical synthesis of single-crystalline $CeOHCO_3$ rods and their thermal conversion to CeO_2 rods," *Nanotechnology*, vol. 16, no. 11, pp. 2502–2506, 2005.

[23] D. E. Zhang, X. M. Ni, H. G. Zheng, X. J. Zhang, and J. M. Song, "Fabrication of rod-like CeO_2: characterization, optical and electrochemical properties," *Solid State Sciences*, vol. 8, no. 11, pp. 1290–1293, 2006.

[24] D. Zhang, H. Fu, L. Shi et al., "Synthesis of CeO_2 nanorods via ultrasonication assisted by polyethylene glycol," *Inorganic Chemistry*, vol. 46, no. 7, pp. 2446–2451, 2007.

[25] F. Gao, Q. Lu, and S. Komarneni, "Fast synthesis of cerium oxide nanoparticles and nanorods," *Journal of Nanoscience and Nanotechnology*, vol. 6, no. 12, pp. 3812–3819, 2006.

[26] Q. Cui, X. Dong, J. Wang, and M. Li, "Direct fabrication of cerium oxide hollow nanofibers by electrospinning," *Journal of Rare Earths*, vol. 26, no. 5, pp. 664–669, 2008.

[27] F. Gu, Z. Wang, D. Han, C. Shi, and G. Guo, "Reverse micelles directed synthesis of mesoporous ceria nanostructures," *Materials Science and Engineering B*, vol. 139, no. 1, pp. 62–68, 2007.

[28] R. J. La, Z. A. Hu, H. L. Li, X. L. Shang, and Y. Y. Yang, "Template synthesis of CeO_2 ordered nanowire arrays," *Materials Science and Engineering A*, vol. 368, no. 1-2, pp. 145–148, 2004.

[29] G. J. Wilson, A. S. Matijasevich, D. R. G. Mitchell, J. C. Schulz, and G. D. Will, "Modification of TiO_2 for enhanced surface properties: finite ostwald ripening by a microwave hydrothermal process," *Langmuir*, vol. 22, no. 5, pp. 2016–2027, 2006.

[30] M. Halder, "Determination of the critical micellar concentration (CMC) of a cationic micelle from stokes shift data," *The Chemical Educator*, vol. 12, no. 1, pp. 33–36, 2007.

[31] R. J. Hunter, *Fundamentals of Colloid Science*, vol. 1-2, Clarendon, Oxford, UK, 1989.

[32] C. Pan, D. Zhang, L. Shi, and J. Fang, "Template-free synthesis, controlled conversion, and CO oxidation properties of CeO_2 nanorods, nanotubes, nanowires, and nanocubes," *European Journal of Inorganic Chemistry*, no. 15, pp. 2429–2436, 2008.

[33] S. Yang and L. Gao, "Controlled synthesis and self-assembly of CeO_2 nanocubes," *Journal of the American Chemical Society*, vol. 128, no. 29, pp. 9330–9331, 2006.

[34] P. W. Atkins, *Physical Chemistry*, Freeman, 1998.

[35] K. Kalyanasundaram, *Photochemistry in Microheterogeneous Systems*, 1987.

[36] D. Terribile, A. Trovarelli, J. Llorca, C. De Leitenburg, and G. Dolcetti, "The synthesis and characterization of mesoporous high-surface area ceria prepared using a hybrid organic/inorganic route," *Journal of Catalysis*, vol. 178, no. 1, pp. 299–308, 1998.

[37] M. Yada, S. Sakai, T. Torikai, T. Watari, S. Furuta, and H. Katsuki, "Cerium compound nanowires and nanorings templated by mixed organic molecules," *Advanced Materials*, vol. 16, no. 14, pp. 1222–1226, 2004.

[38] C. Sun, H. Li, Z. Wang, L. Chen, and X. Huang, "Synthesis and characterization of polycrystalline CeO_2 nanowires," *Chemistry Letters*, vol. 33, no. 6, pp. 662–663, 2004.

[39] L. Yan, X. Xing, R. Yu, J. Deng, J. Chen, and G. Liu, "Facile alcohothermal synthesis of large-scale ceria nanowires with organic surfactant assistance," *Physica B*, vol. 390, no. 1-2, pp. 59–64, 2007.

[40] R. Yang and L. Guo, "Synthesis of cubic fluorite CeO nanowires," *Journal of Materials Science*, vol. 40, pp. 1305–1307, 2005.

[41] D. Zhang, L. Huang, J. Zhang, and L. Shi, "Facile synthesis of ceria rhombic microplates," *Journal of Materials Science*, vol. 43, no. 16, pp. 5647–5650, 2008.

[42] Z. Guo, F. Du, G. Li, and Z. Cui, "Synthesis and characterization of single-crystal $Ce(OH)CO_3$ and CeO_2 triangular microplates," *Inorganic Chemistry*, vol. 45, no. 10, pp. 4167–4169, 2006.

[43] C. S. Riccardi, R. C. Lima, M. L. dos Santos, P. R. Bueno, J. A. Varela, and E. Longo, "Preparation of CeO_2 by a simple microwave-hydrothermal method," *Solid State Ionics*, vol. 180, no. 2-3, pp. 288–291, 2009.

[44] Y. Ikuma, H. Oosawa, E. Shimada, and M. Kamiya, "Effect of microwave radiation on the formation of $Ce_2O(CO_3)_2 \cdot H_2O$ in aqueous solution," *Solid State Ionics*, vol. 151, no. 1–4, pp. 347–352, 2002.

[45] S. Komarneni, Q. H. Li, and R. Roy, "Microwave-hydrothermal processing for synthesis of layered and network

phosphates," *Journal of Materials Chemistry*, vol. 4, no. 12, pp. 1903–1906, 1994.

[46] S. Komarneni, R. Pidugu, Q. H. Li, and R. Roy, "Microwave-hydrothermal processing of metal powders," *Journal of Materials Research*, vol. 10, no. 7, pp. 1687–1692, 1995.

[47] S. Komarneni, R. Roy, and Q. H. Li, "Microwave-hydrothermal synthesis of ceramic powders," *Materials Research Bulletin*, vol. 27, no. 12, pp. 1393–1405, 1992.

[48] C. H. Lu and H. C. Wang, "Formation and microstructural variation of cerium carbonate hydroxide prepared by the hydrothermal process," *Materials Science and Engineering B*, vol. 90, no. 1-2, pp. 138–141, 2002.

[49] Y. Tao, F. H. Gong, H. Wang, H. P. Wu, and G. L. Tao, "Microwave-assisted preparation of cerium dioxide nanocubes," *Materials Chemistry and Physics*, vol. 112, no. 3, pp. 973–976, 2008.

[50] R. Yang and L. Guo, "Synthesis of the nanotublar cubic fluorite CeO_2," *Chinese Journal of Inorganic Chemistry*, vol. 20, no. 2, pp. 152–158, 2004.

[51] S. C. Kuiry, S. D. Patil, S. Deshpande, and S. Seal, "Spontaneous self-assembly of cerium oxide nanoparticles to nanorods through supraaggregate formation," *Journal of Physical Chemistry B*, vol. 109, no. 15, pp. 6936–6939, 2005.

[52] M. Lundberg, B. Skårman, F. Cesar, and L. Reine Wallenberg, "Mesoporous thin films of high-surface-area crystalline cerium dioxide," *Microporous and Mesoporous Materials*, vol. 54, no. 1-2, pp. 97–103, 2002.

[53] J. H. Son, S. W. Kim, D. S. Bae et al., "Synthesis and characterization of CeO_2-doped SiO_2 nanoparticles by a reverse micelle and sol-gel processing," *Materials Science and Engineering A*, vol. 498, no. 1-2, pp. 2–4, 2008.

[54] L. Qian, J. Zhu, W. Du, and X. Qian, "Solvothermal synthesis, electrochemical and photocatalytic properties of monodispersed CeO_2 nanocubes," *Materials Chemistry and Physics*, vol. 115, no. 2-3, pp. 835–840, 2009.

[55] A. Bouchara, G. J. D. A. A. Soler-Illia, J. Y. Chane-Ching, and C. Sanchez, "Nanotectonic approach of the texturation of CeO_2 based nanomaterials," *Chemical Communications*, no. 11, pp. 1234–1235, 2002.

[56] X. Y. Zhang, T. W. Wang, W. Q. Jiang, D. Wu, L. Liu, and A. H. Duan, "Preparation and characterization of three-dimensionally ordered crystalline macroporous CeO_2," *Chinese Chemical Letters*, vol. 16, no. 8, pp. 1109–1112, 2005.

[57] D. Andreescu, E. Matijević, and D. V. Goia, "Formation of uniform colloidal ceria in polyol," *Colloids and Surfaces A*, vol. 291, no. 1–3, pp. 93–100, 2006.

[58] N. Uekawa, M. Ueta, Y. J. Wu, and K. Kakegawa, "Synthesis of CeO_2 spherical fine particles by homogeneous precipitation method with polyethylene glycol," *Chemistry Letters*, no. 8, pp. 854–855, 2002.

[59] N. Uekawa, M. Ueta, Y. J. Wu, and K. Kakegawa, "Characterization of CeO_2 fine particles prepared by the homogeneous precipitation method with a mixed solution of ethylene glycol and polyethylene glycol," *Journal of Materials Research*, vol. 19, no. 4, pp. 1087–1092, 2004.

[60] Z. Yang, L. Liu, H. Liang, H. Yang, and Y. Yang, "One-pot hydrothermal synthesis of CeO_2 hollow microspheres," *Journal of Crystal Growth*, vol. 312, no. 3, pp. 426–430, 2010.

[61] J. M. Herrmann, C. Hoang-Van, L. Dibansa, and R. Harivololona, "An in situ electrical conductivity study of a CeO_2 aerogel supported palladium catalyst in correlation with the total oxidation of propane," *Journal of Catalysis*, vol. 159, no. 2, pp. 361–367, 1996.

[62] C. Laberty-Robert, J. W. Long, E. M. Lucas et al., "Sol-gel-derived ceria nanoarchitectures: synthesis, characterization, and electrical properties," *Chemistry of Materials*, vol. 18, no. 1, pp. 50–58, 2006.

[63] J. L. Gasser-Ramirez, B. C. Dunn, D. W. Ramirez et al., "A simple synthesis of catalytically active, high surface area ceria aerogels," *Journal of Non-Crystalline Solids*, vol. 354, no. 52–54, pp. 5509–5514, 2008.

[64] R. O. Fuentes, L. M. Acuña, M. G. Zimicz et al., "Formation and structural properties of Ce-Zr mixed oxide nanotubes," *Chemistry of Materials*, vol. 20, no. 23, pp. 7356–7363, 2008.

[65] G. Chen, S. Sun, X. Sun, W. Fan, and T. You, "Formation of CeO_2 nanotubes from $Ce(OH)CO_3$ nanorods through kirkendall diffusion," *Inorganic Chemistry*, vol. 48, no. 4, pp. 1334–1338, 2009.

[66] D. Zhang, H. Fu, L. Shi, J. Fang, and Q. Li, "Carbon nanotube assisted synthesis of CeO_2 nanotubes," *Journal of Solid State Chemistry*, vol. 180, no. 2, pp. 654–660, 2007.

[67] J. Fang, Z. Cao, D. Zhang, X. Shen, W. Ding, and L. Shi, "Preparation and CO conversion activity of ceria nanotubes by carbon nanotubes templating method," *Journal of Rare Earths*, vol. 26, no. 2, pp. 153–157, 2008.

[68] D. Zhang, C. Pan, J. Zhang, and L. Shi, "Solvothermal synthesis of necklace-like carbon nanotube/ceria composites," *Materials Letters*, vol. 62, no. 23, pp. 3821–3823, 2008.

[69] Y. Li, J. Ding, J. Chen et al., "Preparation of ceria nanoparticles supported on carbon nanotubes," *Materials Research Bulletin*, vol. 37, no. 2, pp. 313–318, 2002.

[70] J. Wei, J. Ding, X. Zhang et al., "Coated double-walled carbon nanotubes with ceria nanoparticles," *Materials Letters*, vol. 59, no. 2-3, pp. 322–325, 2005.

[71] D. Zhang, L. Shi, H. Fu, and J. Fang, "Ultrasonic-assisted preparation of carbon nanotube/cerium oxide composites," *Carbon*, vol. 44, no. 13, pp. 2853–2855, 2006.

[72] H. X. Fu, D. S. Zhang, L. Y. Shi, and J. H. Fang, "Synthesis and characterization of cerium oxide nanotubes based on carbon nanotubes," *Gaodeng Xuexiao Huaxue Xuebao*, vol. 28, no. 4, pp. 617–620, 2007.

[73] D. Zhang, C. Pan, L. Shi, L. Huang, J. Fang, and H. Fu, "A highly reactive catalyst for CO oxidation: CeO_2 nanotubes synthesized using carbon nanotubes as removable templates," *Microporous and Mesoporous Materials*, vol. 117, no. 1-2, pp. 193–200, 2009.

[74] D. Zhang, T. Yan, L. Shi, C. Pan, and J. Zhang, "Ethylene glycol reflux synthesis of carbon nanotube/ceria core-shell nanowires," *Applied Surface Science*, vol. 255, no. 11, pp. 5789–5794, 2009.

[75] S. C. Laha and R. Ryoo, "Synthesis of thermally stable mesoporous cerium oxide with nanocrystalline frameworks using mesoporous silica templates," *Chemical Communications*, vol. 9, no. 17, pp. 2138–2139, 2003.

[76] W. Shen, X. Dong, Y. Zhu, H. Chen, and J. Shi, "Mesoporous CeO_2 and CuO-loaded mesoporous CeO_2: synthesis, characterization, and CO catalytic oxidation property," *Microporous and Mesoporous Materials*, vol. 85, no. 1-2, pp. 157–162, 2005.

[77] I. A. Kartsonakis, P. Liatsi, I. Daniilidis, and G. Kordas, "Synthesis, characterization, and antibacterial action of hollow ceria nanospheres with/without a conductive polymer coating," *Journal of the American Ceramic Society*, vol. 91, no. 2, pp. 372–378, 2008.

[78] I. Kartsonakis, I. Daniilidis, and G. Kordas, "Encapsulation of the corrosion inhibitor 8-hydroxyquinoline into ceria nanocontainers," *Journal of Sol-Gel Science and Technology*, vol. 48, no. 1, pp. 24–31, 2008.

[79] G. S. Wu, T. Xie, X. Y. Yuan, B. C. Cheng, and L. D. Zhang, "An improved sol-gel template synthetic route to large-scale CeO_2 nanowires," *Materials Research Bulletin*, vol. 39, no. 7-8, pp. 1023–1028, 2004.

[80] D. E. Zhang, X. J. Zhang, X. M. Ni, J. M. Song, and H. G. Zheng, "Optical and electrochemical properties of CeO_2 spindles," *ChemPhysChem*, vol. 7, no. 12, pp. 2468–2470, 2006.

[81] M. Hirano and E. Kato, "Hydrothermal synthesis of two types of cerium carbonate particles," *Journal of Materials Science Letters*, vol. 18, no. 5, pp. 403–405, 1999.

[82] H. C. Wang and C. H. Lu, "Synthesis of cerium hydroxy-carbonate powders via a hydrothermal technique," *Materials Research Bulletin*, vol. 37, no. 4, pp. 783–792, 2002.

[83] M. Ge, C. Guo, L. Li, B. Zhang, Y. Feng, and Y. Wang, "Preparation of CeO_2 novel sponge-like rods by emulsion liquid membrane system and its catalytic oxidation property," *Materials Letters*, vol. 63, no. 15, pp. 1269–1271, 2009.

[84] A. G. Macedo, S. E. M. Fernandes, A. A. Valente, R. A. S. Ferreira, L. D. Carlos, and J. Rocha, "Catalytic performance of ceria nanorods in liquid-phase oxidations of hydrocarbons with tert-butyl hydroperoxide," *Molecules*, vol. 15, no. 2, pp. 747–765, 2010.

[85] X. He, D. Zhang, H. Li, J. Fang, and L. Shi, "Shape and size effects of ceria nanoparticles on the impact strength of ceria/epoxy resin composites," *Particuology*, 2010.

[86] J. J. Miao, H. Wang, Y. R. Li, J. M. Zhu, and J. J. Zhu, "Ultrasonic-induced synthesis of CeO_2 nanotubes," *Journal of Crystal Growth*, vol. 281, no. 2–4, pp. 525–529, 2005.

[87] M. L. Dos Santos, R. C. Lima, C. S. Riccardi et al., "Preparation and characterization of ceria nanospheres by microwave-hydrothermal method," *Materials Letters*, vol. 62, no. 30, pp. 4509–4511, 2008.

[88] W. Q. Han, L. Wu, and Y. Zhu, "Formation and oxidation state of CeO_{2-x} nanotubes," *Journal of the American Chemical Society*, vol. 127, no. 37, pp. 12814–12815, 2005.

[89] C. Tang, Y. Bando, B. Liu, and D. Golberg, "Cerium oxide nanotubes prepared from cerium hydroxide nanotubes," *Advanced Materials*, vol. 17, no. 24, pp. 3005–3009, 2005.

[90] G. Chen, C. Xu, X. Song, W. Zhao, Y. Ding, and S. Sun, "Interface reaction route to two different kinds of CeO_2 nanotubes," *Inorganic Chemistry*, vol. 47, no. 2, pp. 723–728, 2008.

[91] W. Wang, J. Y. Howe, Y. Li et al., "A surfactant and template-free route for synthesizing ceria nanocrystals with tunable morphologies," *Journal of Materials Chemistry*, vol. 20, no. 36, pp. 7776–7781, 2010.

[92] K. Zhou, Z. Yang, and S. Yang, "Highly reducible CeO_2 nanotubes," *Chemistry of Materials*, vol. 19, no. 6, pp. 1215–1217, 2007.

[93] Z. L. Wang and X. Feng, "Polyhedral shapes of CeO_2 nanoparticles," *Journal of Physical Chemistry B*, vol. 107, no. 49, pp. 13563–13566, 2003.

[94] Y. C. Chen, K. B. Chen, C. S. Lee, and M. C. Lin, "Direct synthesis of Zr-doped ceria nanotubes," *Journal of Physical Chemistry C*, vol. 113, no. 13, pp. 5031–5034, 2009.

[95] P. Martin, S. C. Parker, D. C. Sayle, and G. W. Watson, "Atomistic modeling of multilayered ceria nanotubes," *Nano Letters*, vol. 7, no. 3, pp. 543–546, 2007.

[96] Y. Fu, Z. D. Wei, M. B. Ji, L. Li, P. K. Shen, and J. Zhang, "Morphology-controllable synthesis of CeO_2 on a Pt electrode," *Nanoscale Research Letters*, vol. 3, no. 11, pp. 431–434, 2008.

[97] N. Bugayeva and J. Robinson, "Synthesis of hydrated CeO_2 nanowires and nanoneedles," *Materials Science and Technology*, vol. 23, no. 2, pp. 237–241, 2007.

[98] K. S. Lin, S. Chowdhury, H. P. Yeh, W. T. Hong, and C. T. Yeh, "Preparation and characterization of $CuO/ZnO\text{-}Al_2O_3$ catalyst washcoats with CeO_2 sols for autothermal reforming of methanol in a microreactor," *Catalysis Today*, vol. 164, no. 1, pp. 251–256, 2011.

[99] D. Zhang, T. Yan, C. Pan, L. Shi, and J. Zhang, "Carbon nanotube-assisted synthesis and high catalytic activity of CeO_2 hollow nanobeads," *Materials Chemistry and Physics*, vol. 113, no. 2-3, pp. 527–530, 2009.

[100] T. Masui, K. Fujiwara, K. I. Machida, G. Y. Adachi, T. Sakata, and H. Mori, "Characterization of cerium(IV) oxide ultrafine particles prepared using reversed micelles," *Chemistry of Materials*, vol. 9, no. 10, pp. 2197–2204, 1997.

[101] D. Zhang, F. Niu, H. Li, L. Shi, and J. Fang, "Uniform ceria nanospheres: solvothermal synthesis, formation mechanism, size-control and catalytic activity," *Powder Technology*, vol. 207, no. 1–3, pp. 35–41, 2011.

[102] D. Zhang, F. Niu, T. Yan, L. Shi, X. Du, and J. Fang, "Ceria nanospindles: template-free solvothermal synthesis and shape-dependent catalytic activity," *Applied Surface Science*, vol. 257, no. 23, pp. 10161–10167, 2011.

[103] J. Guzman, S. Carrettin, and A. Corma, "Spectroscopic evidence for the supply of reactive oxygen during CO oxidation catalyzed by gold supported on nanocrystalline CeO_2," *Journal of the American Chemical Society*, vol. 127, no. 10, pp. 3286–3287, 2005.

[104] M. B. Boucher, S. Goergen, N. Yi, and M. Flytzani-Stephanopoulos, "'Shape effects' in metal oxide supported nanoscale gold catalysts," *Physical Chemistry Chemical Physics*, vol. 13, no. 7, pp. 2517–2527, 2011.

[105] K. S. Lin, C. Y. Pan, S. Chowdhury, M. T. Tu, W. T. Hong, and C. T. Yeh, "Hydrogen generation using a $CuO/ZnO\text{-}ZrO_2$ nanocatalyst for autothermal reforming of methanol in a microchannel reactor," *Molecules*, vol. 16, no. 1, pp. 348–366, 2011.

[106] Y. Liu, T. Hayakawa, K. Suzuki, and S. Hamakawa, "Production of hydrogen by steam reforming of methanol over Cu/CeO_2 catalysts derived from $Ce_{1-x}Cu_xO_{2-x}$ precursors," *Catalysis Communications*, vol. 2, no. 6-7, pp. 195–200, 2001.

[107] D. J. Seo, W. L. Yoon, Y. G. Yoon, S. H. Park, G. G. Park, and C. S. Kim, "Development of a micro fuel processor for PEMFCs," *Electrochimica Acta*, vol. 50, no. 2-3, pp. 719–723, 2004.

[108] M. B. Boucher, N. Yi, F. Gittleson, B. Zugic, H. Saltsburg, and M. Flytzani-Stephanopoulos, "Hydrogen production from methanol over gold supported on ZnO and CeO_2 nanoshapes," *Journal of Physical Chemistry C*, vol. 115, no. 4, pp. 1261–1268, 2011.

[109] N. Yi, R. Si, H. Saltsburg, and M. Flytzani-Stephanopoulos, "Steam reforming of methanol over ceria and gold-ceria nanoshapes," *Applied Catalysis B*, vol. 95, no. 1-2, pp. 87–92, 2010.

[110] G. Avgouropoulos, J. Papavasiliou, and T. Ioannides, "Hydrogen production from methanol over combustion-synthesized noble metal/ceria catalysts," *Chemical Engineering Journal*, vol. 154, no. 1–3, pp. 274–280, 2010.

[111] N. Yi, R. Si, H. Saltsburg, and M. Flytzani-Stephanopoulos, "Active gold species on cerium oxide nanoshapes for methanol steam reforming and the water gas shift reactions," *Energy and Environmental Science*, vol. 3, no. 6, pp. 831–837, 2010.

[112] X. Yu, S. T. Tu, Z. Wang, and Y. Qi, "Development of a microchannel reactor concerning steam reforming of methanol," *Chemical Engineering Journal*, vol. 116, no. 2, pp. 123–132, 2006.

[113] P. J. De Wild and M. J. F. M. Verhaak, "Catalytic production of hydrogen from methanol," *Catalysis Today*, vol. 60, no. 1, pp. 3–10, 2000.

[114] X. Yu, S. T. Tu, Z. Wang, and Y. Qi, "On-board production of hydrogen for fuel cells over $Cu/ZnO/Al_2O_3$ catalyst coating in a micro-channel reactor," *Journal of Power Sources*, vol. 150, no. 1-2, pp. 57–66, 2005.

[115] T. Kim, D. H. Lee, D. E. Park, and S. Kwon, "Micromachined methanol reformer for portable PEM fuel cells," *Journal of Fuel Cell Science and Technology*, vol. 5, no. 1, Article ID 011008, 6 pages, 2008.

[116] C. Horny, A. Renken, and L. Kiwi-Minsker, "Compact string reactor for autothermal hydrogen production," *Catalysis Today*, vol. 120, no. 1, pp. 45–53, 2007.

[117] G. Germani, A. Stefanescu, Y. Schuurman, and A. C. van Veen, "Preparation and characterization of porous alumina-based catalyst coatings in microchannels," *Chemical Engineering Science*, vol. 62, no. 18–20, pp. 5084–5091, 2007.

[118] C. G. MacIel, L. P. R. Profeti, E. M. Assaf, and J. M. Assaf, "Hydrogen purification for fuel cell using CuO/CeO_2-Al_2O_3 catalyst," *Journal of Power Sources*, vol. 196, no. 2, pp. 747–753, 2011.

[119] G. Avgouropoulos and T. Ioannides, "Selective CO oxidation over CuO-CeO_2 catalysts prepared via the urea-nitrate combustion method," *Applied Catalysis A*, vol. 244, no. 1, pp. 155–167, 2003.

[120] G. G. Park, S. D. Yim, Y. G. Yoon, C. S. Kim, D. J. Seo, and K. Eguchi, "Hydrogen production with integrated microchannel fuel processor using methanol for portable fuel cell systems," *Catalysis Today*, vol. 110, no. 1-2, pp. 108–113, 2005.

[121] D. E. Park, T. Kim, S. Kwon, C. K. Kim, and E. Yoon, "Micromachined methanol steam reforming system as a hydrogen supplier for portable proton exchange membrane fuel cells," *Sensors and Actuators A*, vol. 135, no. 1, pp. 58–66, 2007.

[122] A. Qi, B. Peppley, and K. Karan, "Integrated fuel processors for fuel cell application: a review," *Fuel Processing Technology*, vol. 88, no. 1, pp. 3–22, 2007.

[123] M. S. Lim, M. R. Kim, J. Noh, and S. I. Woo, "A plate-type reactor coated with zirconia-sol and catalyst mixture for methanol steam-reforming," *Journal of Power Sources*, vol. 140, no. 1, pp. 66–71, 2005.

[124] G. Huang, B. J. Liaw, C. J. Jhang, and Y. Z. Chen, "Steam reforming of methanol over $CuO/ZnO/CeO_2/ZrO_2/Al_2O_3$ catalysts," *Applied Catalysis A*, vol. 358, no. 1, pp. 7–12, 2009.